



**HAL**  
open science

# Variation of the first cut-off frequency of the Earth-ionosphere waveguide observed by DEMETER

S Toledo-Redondo, Michel Parrot, A Salinas

► **To cite this version:**

S Toledo-Redondo, Michel Parrot, A Salinas. Variation of the first cut-off frequency of the Earth-ionosphere waveguide observed by DEMETER. *Journal of Geophysical Research Space Physics*, 2012, 117, A04321 (11 p.). 10.1029/2011JA017400 . insu-01179859

**HAL Id: insu-01179859**

**<https://insu.hal.science/insu-01179859>**

Submitted on 23 Jul 2015

**HAL** is a multi-disciplinary open access archive for the deposit and dissemination of scientific research documents, whether they are published or not. The documents may come from teaching and research institutions in France or abroad, or from public or private research centers.

L'archive ouverte pluridisciplinaire **HAL**, est destinée au dépôt et à la diffusion de documents scientifiques de niveau recherche, publiés ou non, émanant des établissements d'enseignement et de recherche français ou étrangers, des laboratoires publics ou privés.

## Variation of the first cut-off frequency of the Earth-ionosphere waveguide observed by DEMETER

S. Toledo-Redondo,<sup>1,2</sup> M. Parrot,<sup>1</sup> and A. Salinas<sup>2</sup>

Received 8 December 2011; revised 9 March 2012; accepted 11 March 2012; published 28 April 2012.

[1] More than four years of VLF electric field data recorded by DEMETER have been analyzed, in order to monitor the first cut-off frequency (QTM<sub>1</sub>) of the Earth-ionosphere waveguide, at around 1.6–1.8 kHz. Since losses in a waveguide are maximized right at the cut-off frequency, DEMETER (~700 km orbit) can detect the minimum of energy of the leaking fields coming from the waveguide. This measurement permits to draw a global map of its value ( $f_1$ ), which is directly related to the effective height of the ionosphere ( $h$ ) by the relation  $f_1 = c/2h$  ( $c$  is the speed of light). It enables the remote sensing of the D region, which is one of the less known layers of the ionosphere, because it is too low for satellites to orbit inside it and too high for balloons to reach it. The effective height depends mainly on the electron density ( $N_e$ ) and neutral density ( $N_n$ ) profiles, which determine the plasma frequency and the electron mobility. The effective height shifts downward 5–10 km in southern warm season in the South Pacific Ocean. Another effect is observed in the Indian and Atlantic Oceans; the effective height decreases its value twice a year, in the area of roughly  $\pm 15^\circ$  from the geomagnetic equator. The main causes for the changes on the effective reflection height are the solar radiation and the thunderstorm activity. However, the observed shifts are more prominent over the oceans, and a possible explanation for this difference could be attributed to i) less polluted conditions above the oceans (aerosols change the atmospheric conductivity and then the global atmospheric electric circuit), ii) the effect of the current associated to the thunderclouds on the bottom of the ionosphere because thunderstorms are much more numerous above land, or iii) ionization by elves because their occurrence is larger above oceans.

**Citation:** Toledo-Redondo, S., M. Parrot, and A. Salinas (2012), Variation of the first cut-off frequency of the Earth-ionosphere waveguide observed by DEMETER, *J. Geophys. Res.*, 117, A04321, doi:10.1029/2011JA017400.

### 1. Introduction

[2] The surface of the Earth and the lower ionosphere are both conductive in the ELF-VLF bands. The gap between the two conductive spheres contains air and it is known as the atmosphere. When considered as a whole, we talk about the Earth-ionosphere cavity or waveguide. While the lower boundary of the cavity is sharp and well defined, the conductivity increases with height at the upper boundary. It mainly depends on the electron and neutral density profiles, which are affected by several parameters such as local time, solar activity index, or geomagnetic field [Hargreaves, 1992].

[3] Due to the geometry of the cavity, i.e. large but thin, it behaves in different manner for different frequency ranges of waves, originated mainly due to thunderstorms. In the ELF

band, where the wavelength ( $\lambda$ ) is on the order of the Earth's circumference, it acts as a resonator, accommodating standing waves which are present in the whole cavity. These are the well known Schumann Resonances (SR) [Schumann, 1952; Nickolaenko and Hayakawa, 2002], which correspond to QTM modes of the cavity. In addition, it also behaves as a waveguide in the VLF band, where  $\lambda$  is on the order of the separation  $h$  between the two conductive spheres. This wave-guiding effect can be approximated, on a first approach, by conducting parallel plates. This effect is local and the generated signals travel a certain distance from the source before vanishing due to losses. These signals in the waveguide are known as atmospherics, or sferics [Barr et al., 2000; Hayakawa et al., 1994]. Sferics suffer multiple reflections between the two conductive spheres, and its  $n$ -th mode cut-off frequency can be related, according to Cheng [1989], to the effective height of the ionosphere ( $h$ ) by

$$f_n = \frac{nc}{2h} \quad (1)$$

where  $c$  is the speed of light in vacuum,  $n$  is the cut-off frequency mode number, and  $f_n$  the associated cut-off frequency

<sup>1</sup>Laboratoire de Physique et Chimie de l'Environnement et de l'Espace, CNRS, Orléans, France.

<sup>2</sup>Department of Electromagnetism and Matter Physics, University of Granada, Granada, Spain.

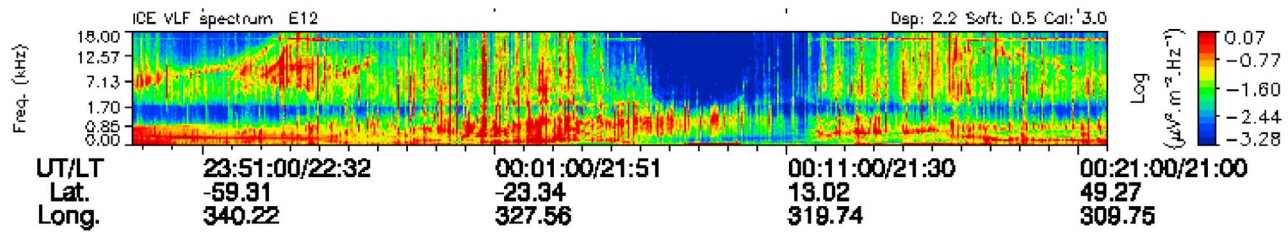


**Figure 1.** ICE-VLF spectrogram of a nighttime half orbit recorded by DEMETER. It corresponds to October 1, 2010, over the Atlantic Ocean. The cut-off frequency of the Earth-ionosphere cavity can be clearly seen at around 1.7 kHz.

of the mode. The first cut-off frequency is around 1.7 kHz, corresponding to an effective height of  $\sim 90$  km. They were estimated for the first time by *Bliokh et al.* [1977], and their experimental detection was described by *Lazebny et al.* [1988].

[4] Below the cut-off frequency only the QTEM mode can propagate. For frequencies above the cut-off the QTM<sub>1</sub> mode also propagates, its attenuation being maximum right at the cut-off frequency [*Ramo et al.*, 1994]. Therefore, there is a detectable minimum of energy in the atmospheric spectrum for this frequency. *Cummer* [2000] employed the numerical method of Finite Differences in Time Domain, or FDTD [*Taflove and Hagness*, 2005], in order to simulate sferics propagation in the Earth-ionosphere waveguide, his results being consistent with this minimum of energy at the cut-off frequency.

[5] Monitoring these cut-off frequencies can provide valuable information about the waveguide properties since it is a tool to effectively remote sensing the lower D-region of the ionosphere [*Ryabov*, 1992; *Cummer et al.*, 1998]. Direct relation between the cut-off frequency and the electron density is shown by *Shvets and Hayakawa* [1997] and *Ohya et al.* [2003]. This region of the ionosphere is one of the less observed regions. In-situ measurements could not be done due to the fact that it is too high to be reached by balloons and too low for satellite orbits. However, information can be obtained by remote sensing which is done with satellites as well as with ground-based radars, natural or man-made VLF waves, and optical measurements [e.g., *Cummer et al.*, 1998].

[6] The principal source of excitation of the cavity at these frequencies is lightning. This fact enables the interest of studying the resonances for global climate analysis [*Williams*, 1992], and, since they contain information of thunderstorm activity [*Toledo-Redondo et al.*, 2010], they can be a tool to study thunderstorms and the dynamics related to them.

[7] In this paper, the first cut-off frequency of the Earth-ionosphere waveguide is analyzed by means of more than four years of DEMETER ICE (*Instrument Champ Electrique*, or Electric Field Instrument) experiment data. The experiment is presented in section 2, and the analysis procedures are detailed in sections 3 and 4. A month by month analysis reveals seasonal patterns repeating in all the years for the cut-off frequency at certain geographical locations. Maps showing the cut-off frequency value at all the globe as well as descriptions for the found patterns are presented in section 5. The mechanisms that may originate the cut-off

frequency drifts are discussed in section 6. In section 7, the main conclusions of this paper are summarized.

## 2. VLF Electric Field Measurements on DEMETER

[8] DEMETER is a French scientific micro satellite, the first of the MYRIADE series [*Cussac et al.*, 2006]. It was launched in June 2004 with the principal purpose of studying ionosphere precursors of earthquakes. It has a nearly circular sun-synchronous orbit and the upgoing half-orbits correspond to nighttime (22.30 LT) whereas the down-going half-orbits correspond to day time (10.30 LT). This means that all measurements of DEMETER were performed either at roughly 22.30 LT or 10.30 LT, regardless of the latitude or orbit number. Its polar orbit has an inclination of  $98^\circ$ . Its initial altitude was 710 km but it was changed by the ground mission to 660 km in December 2005. It performs 14 orbits per day and gathers data for geomagnetic invariant latitudes between  $\pm 65^\circ$ . The time that the satellite is out of this latitude is used for maintenance. The satellite operates in two modes; survey and burst. Burst mode is only activated when the satellite is over sensible earthquake areas. During burst mode, the whole time series of the instruments are sent to the mission center, together with the on board computed spectra. During survey mode, only spectra is sent. Its scientific payload consists of electric field sensor (ICE), magnetic search coil (IMSC), Langmuir probe (ISL), plasma analyzer (IAP), and energetic particle detector (IDP).

[9] ICE is composed of four spherical electrodes with embedded pre-amplifiers, which are deployed at 4 meters each from the spacecraft by stacer booms. The signal processing and A/D conversion is subdivided in four channels: DC/ULF (0–15 Hz), ELF (15 Hz–1 kHz), VLF (15 Hz–17.4 kHz), and HF (10 kHz–3.175 MHz). In this study only VLF signals have been considered. The sampling frequency is therefore 40 kHz and the samples are digitized using 16 bits. The sensitivity of the sensors at this frequency range is  $\sim 0.05 \mu\text{V m}^{-1} \text{Hz}^{-1/2}$  [*Berthelier et al.*, 2006]. Spectra of 19.53 Hz resolution are computed on board, and averaged in groups of 40, leading to a time resolution of 2.048 s. These averaged spectra are normalized to its maximum, converted to 8 bits resolution and telemetered to ground. In VLF operation mode, only one component of the electric field is sent to the Earth during survey mode. For the years of this study (2006–2010), this component was always  $E_{12}$ , which is roughly parallel to the East-West direction on Earth.

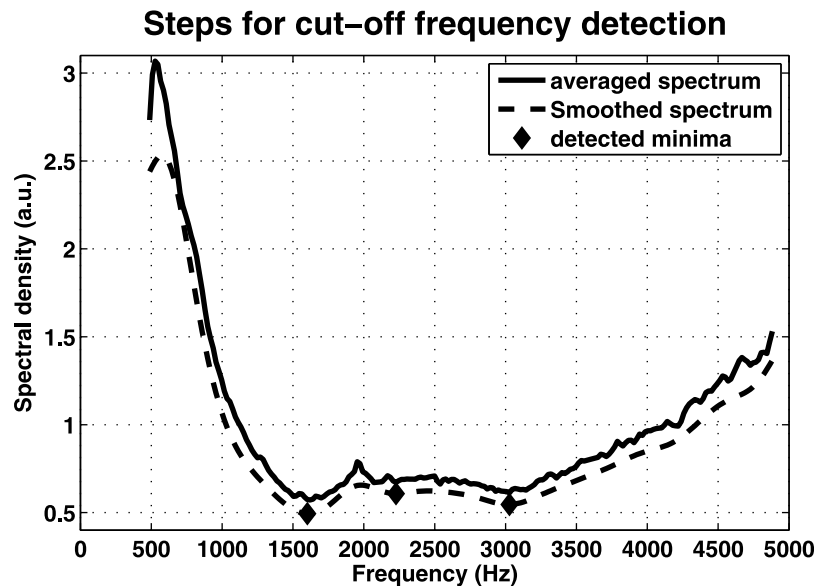


**Figure 2.** Example of the steps involved in minima detection. The linear averaged spectrum is first smoothed by applying the FIR LPF, then an algorithm finds the local minima of the resulting spectrum.

[10] In this work, more than 4 years data (2006, 2007, 2008, 2009 and part of 2010) from ICE in survey mode were used. Only nighttime spectra, pertaining to the VLF range, were considered. It corresponds with more than 20000 DEMETER orbits. During the chosen years the solar activity is known to be low, specially during the last years. The ionosphere conditions are very different between day and nighttime, the day time being a much more complex situation because, on one hand, the intensity of the natural noise (mainly hiss) is much more important and, on the other hand, the intensity of the sferics is highly attenuated due to the increased density in the ionosphere. Therefore, day time ICE data were not used in this study. Two levels of data are available from the servers [Lagoutte *et al.*, 2006]; level 0 corresponds to raw data, as sent by the spacecraft, and level 1 corresponds to calibrated data. Level 1 VLF ICE survey mode data is comprised of spectral lines with 19.5 Hz resolution, the spacecraft sending one spectrum every 2.048 s [Lagoutte *et al.*, 2005]. Due to the Sun-synchronous orbit, the spectra correspond always to roughly 22.30 LT. An example of the data can be seen in Figure 1, where the received ICE-VLF spectrogram of DEMETER for one half-orbit is depicted. The cut-off frequency is clearly distinguishable at around 1.7 kHz.

### 3. Cut-Off Frequency Detection

[11] The cut-off frequency of the Earth-Ionosphere waveguide is seen by DEMETER as a minimum of energy. Electric field energy radiated from the atmosphere (originated primarily by lightning at the range of kHz) crosses the lower ionosphere up to the orbit of DEMETER. Since the losses are maximized at the cut-off frequency of the waveguide, the spectra contains a minimum of energy right at its effective value. We have focused on detecting this minimum of energy, which is present in almost all spectra from nighttime orbits.

[12] In order to accomplish that, first we have to decide the time span that we want to average, for instance one month or one year. Then a geographical grid step must be chosen. In our analysis we are considering spectra recorded between  $\pm 60^\circ$ , and grid steps between  $1-5^\circ$ . Once the grid and the time span are defined, for each cell of the grid we take all the nighttime spectra available on the DEMETER database. The Level 1 VLF-ICE spectra are in  $\log(\mu\text{V}^2\text{m}^{-2}\text{Hz}^{-1})$ . We first linearize them, then each spectrum is normalized to its mean. Finally, all the spectra which belong to the same spatial and temporal grid cell are averaged.

[13] Once we have reduced all the data to one single averaged spectrum per grid cell, it is smoothed by a zero phase shift Low-pass Filter (LPF) [Onishi and Berthelier, 2010]. The filter is a digital FIR of 48 samples, which attenuates 60 dB in its attenuated band. Its band pass is up to 0.075 (normalized to 1), and its attenuated band starts at 0.175. The filtering is performed in order to be able to automatically detect the position of the significant local minima of the spectra.

[14] Once we have a smoothed curve for each cell, an automatic finding of local minima is performed (see Figure 2), by comparing the value of each sample with its nearby samples. The found minima are divided in two groups; those which are below 1.4 kHz and those which are above, the first group being discarded. If there is more than one local minimum in the interval 1.4–2.0 kHz, or the first minimum is above this range, the cut-off frequencies detected are considered to be invalid. Otherwise the minimum is considered to be the cut-off frequency for the corresponding cell.

### 4. Calculation of Electron Density at the Effective Height

[15] The technique described above permits to obtain the value of the first cut-off frequency for an arbitrary area of the

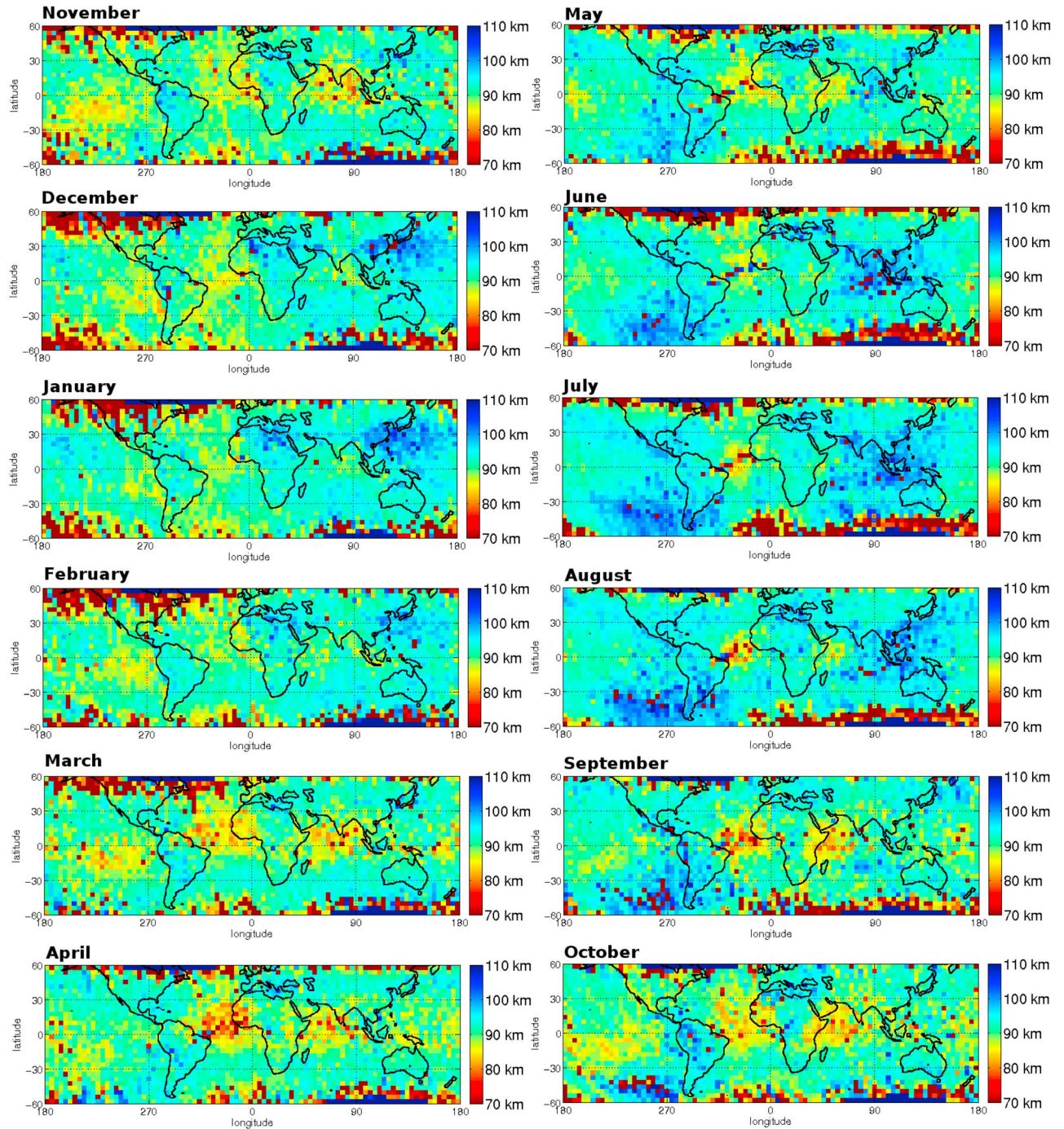


**Figure 3.** Map of the effective reflection height for different months averaged among four years. (left) Northern cold season (November to April) and (right) northern warm season (May to October). The height is color-coded according to the scale in km on the right.

globe, and for an arbitrary time span. As it is shown in equation (1), the effective reflection height can be obtained from the cut-off frequency. It is possible from these values to infer the electron density at the effective height. In order to do that, it is necessary to know the neutral density ( $N_n$ ) at the altitude of interest. This parameter has been extracted from the empirical model MSIS [Labitzke *et al.*, 1985; Hedin, 1991].

[16] Following Ratcliffe [1959], the reflection of the wave in the ionosphere occurs when

$$f_p^2 = f\nu \quad (2)$$

where  $f_p$  is the plasma frequency,  $f$  is the frequency of the wave, and  $\nu$  is the collision frequency of the

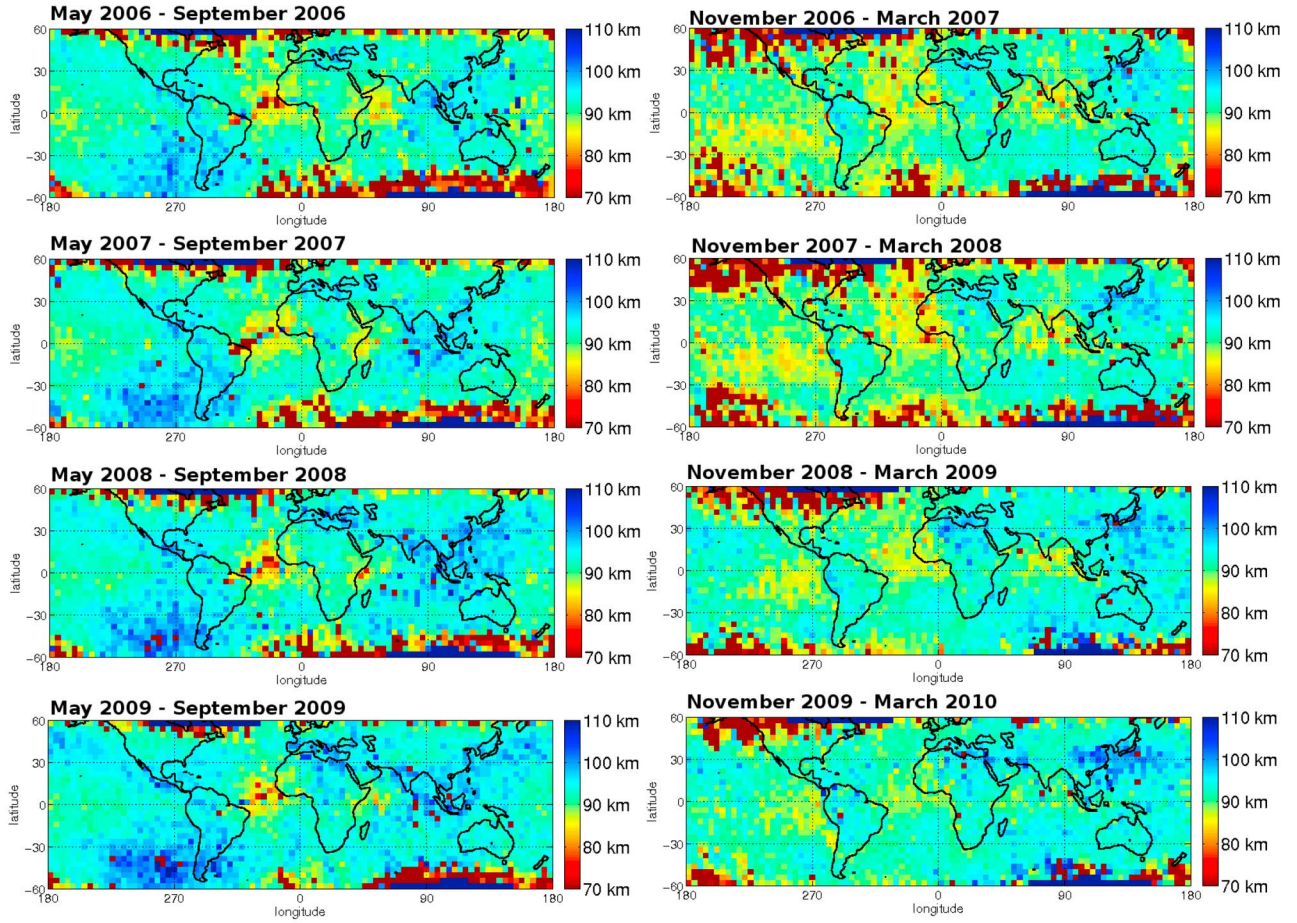


**Figure 4.** Map of the effective reflection height for different seasons and years. The height is color-coded according to the scale in km on the right. (left) Northern warm season and (right) northern cold season. A seasonal effect which repeats every year can be observed. The effect is a shift on the cut-off frequency, and therefore in the effective reflection height, which occurs over the Pacific Ocean. It can also be observed that reflection height is lower at equatorial Atlantic and Indian Oceans.

plasma. This last parameter depends only on the electron mobility  $\mu_e$

$$\nu = \frac{q_e}{m_e \mu_e} \quad (3)$$

where  $q_e$  is the electron charge and  $m_e$  its mass. In Pasko *et al.* [1997], the following expression relating the electron mobility to the density of neutrals is given:

$$\mu_e = \frac{1.36 N_0}{N_n} \quad (4)$$

where  $N_0$  is  $2.688 \cdot 10^{25} \text{ m}^{-3}$  and  $N_n$  is the neutral density. This expression will be used to obtain the collision frequency from the neutral density given by the MSIS model. Then, the electron density ( $N_e$ ) at the effective height can be inferred from

$$f_p \approx 8980 \sqrt{N_e} \quad (5)$$

where  $f_p$  is the plasma frequency in Hz and  $N_e$  the electron density in  $\text{cm}^{-3}$ . This expression is valid for cold plasmas [Ratcliffe, 1959]. With this method, it is possible to interpret the effective height in terms of

ionospheric electron density. Finally, the effective conductivity ( $\sigma_e$ ) at the reflection height can also be obtained:

$$\sigma_e = q_e N_e \mu_e \quad (6)$$

## 5. Results

[17] A data set of four years plus two months (in order to have complete seasons) has been analyzed with the technique described in previous section. We examined the data month by month along the time span and found certain patterns repeating in correlative months as well as in the same months for all the years. In Figure 3 we have averaged the data of equal months along the four years. The averaged year evolution reveals different effects of the effective height for different geographical areas. In general terms, the effective height is of a lower value for the northern hemisphere cold season, i.e. roughly from November to March. This shift is more prominent at the ocean, but it can be observed in land areas as well, with the great exception of Eastern Asia and Western Pacific Ocean, where no shift can be appreciated with seasons. The shift is on the order of 5–10 km,

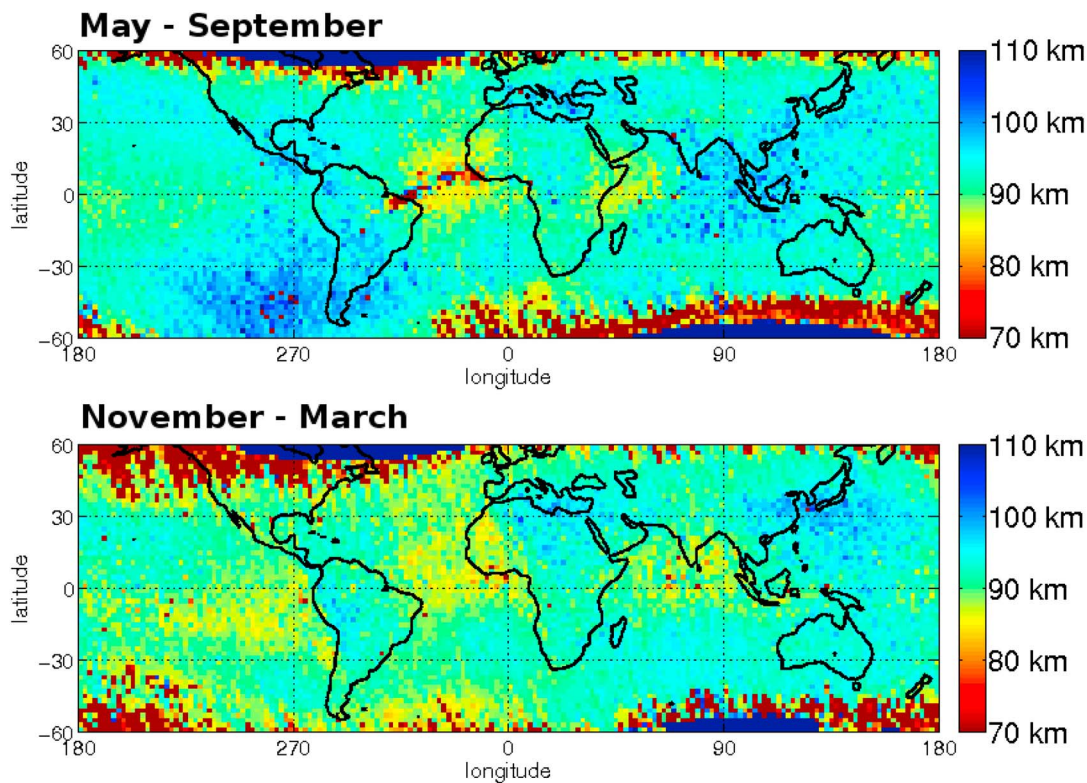


**Figure 5.** Map of the effective reflection height for the averaged seasons among four years. (top) Data of May–September of years 2006, 2007, 2008 and 2009. (bottom) Data from northern winters of 2006, 2007, 2008, 2009 and first months of 2010. Northern winter, for this study, is considered to start in November and last till March. The height is color-coded according to the scale in km on the right.

corresponding to a cut-off frequency shift of 100–200 Hz (see Figures 4 and 5).

[18] The most clear seasonal effect is produced in the Pacific Ocean only for the Southern Hemisphere, for the geographical area roughly comprised on latitudes  $-60^{\circ}$  to  $0^{\circ}$  and longitudes  $180^{\circ}$  to  $280^{\circ}$ . In this area, at high latitudes the effective height takes values higher than 100 km between May and October. From November to April in the same region the effective height decreases to  $\sim 90$  km. For lower latitudes ( $-30^{\circ}$  to  $0^{\circ}$ ) the effect is similar but the global value of the effective height is lower. Between May and October the value is around  $\sim 90$  km, and decreasing to  $\sim 85$  km between November and April.

[19] Another interesting phenomenon occurs at equatorial latitudes, for both Atlantic and Indian Oceans. Although these two areas are geographically separated by African continent, they shift their cut-off frequency, and therefore their effective height, accordingly. For these areas the shift appears not once but twice a year. The effective height presents a low value (around 88 km) at the center of the disturbances during all months, with their centers roughly located at  $(0^{\circ}\text{N}, 340^{\circ})$ , and  $(0^{\circ}\text{N}, 80^{\circ})$  respectively. The low effective height area considerably increases during March–April, and again during September–October, comprising a total area of 2–4 times larger than the one of the rest of the year.

[20] In Figure 3 several red points can be noticed. They correspond to points out of the scale, and they can occur

under two different situations. The first is that our algorithm found the first minimum in the spectrum above 2.0 kHz. The other case is that the algorithm found more than two significant local minima in the interval 1.4–2.0 kHz. In both cases we understand the event as a non detectable first cut-off frequency, and therefore we could not infer the effective height of reflection.

[21] This automatic detection of minimum frequency in the DEMETER VLF spectra fails when the intensity of the natural waves coming from above the satellite exceeds the intensity of the whistler waves which propagate in the Earth-ionosphere waveguide. It can be seen in Figure 3 that it occurs mainly at high latitudes where intense waves such as VLF auroral hiss, chorus, lower hybrid electrostatic noise, etc. are predominant. It is interesting to note that the Atlantic Ocean region between Brazil and Cape Verde exhibits also such problem (mainly during summer time). The reason is that it corresponds to the inter-tropical convergence zone where the ionosphere is highly variable and presents a maximum of plasma bubbles [Kil and Heelis, 1998; Su et al., 2006]. At this location, DEMETER records a very disturbed electric field.

[22] We have grouped the months in order to better see the effective height shift in the Pacific Ocean. For each year we have averaged two periods: May–September (southern cold season) and November–March (southern warm season). The results are shown in Figure 4. For each individual year the shift between seasons can be observed, and its value and

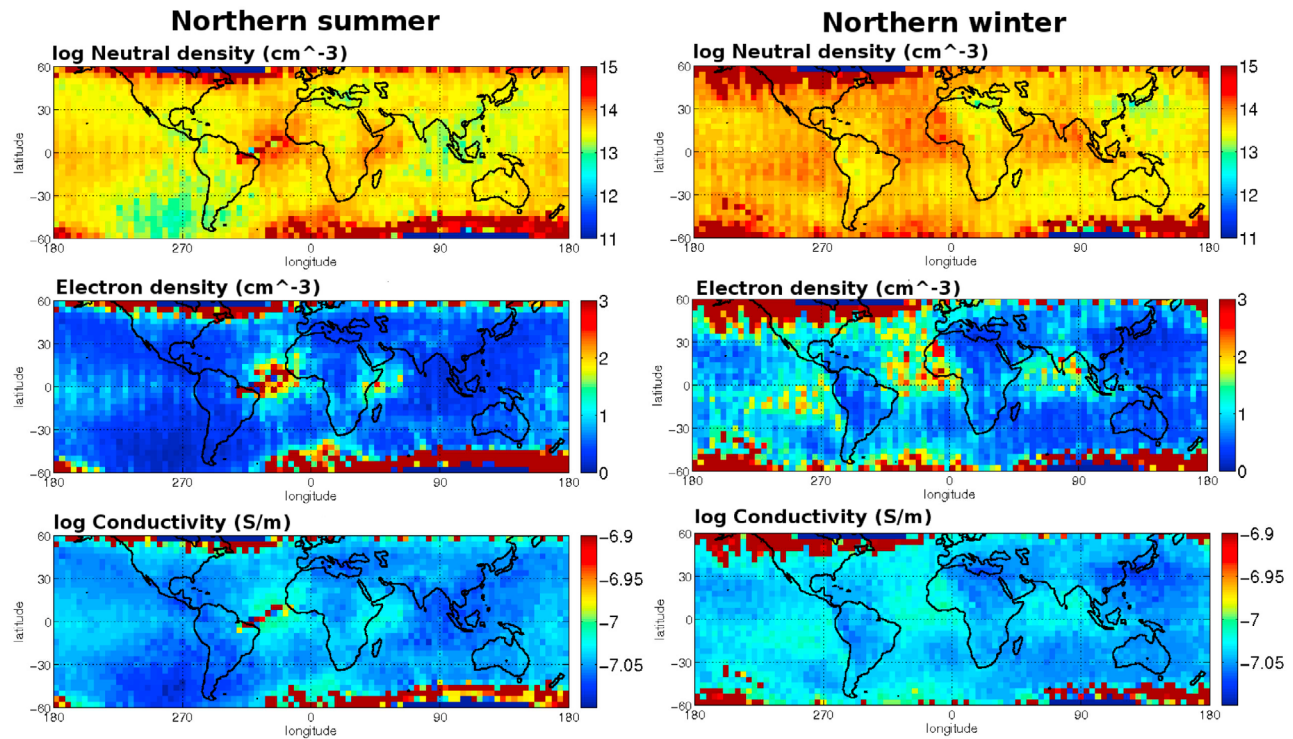


**Figure 6.** Maps of neutral density, electron density, and conductivity at effective height. The values correspond to the seasonal average (May–September for northern summer and November–March for northern winter) of years 2006–2009. The density of neutrals was obtained from MSIS model for the corresponding effective height shown in Figure 5. Then, the electron density and the conductivity are calculated as explained in section 4.

location are very similar. It is interesting to note that the southern warm season shift (toward  $\sim 85$  km) is abruptly disrupted at the western South American coast. On the other hand, for the cold season this effect is not observed.

[23] The previous seasons have been averaged and grouped in just two blocks; northern warm season and northern cold season (see Figure 5). The Pacific Ocean effective height shift can be observed. In addition, the northern winter panel (Figure 5, bottom) reveals that the effective height is a bit lower around the geomagnetic equator for most of the ocean areas.

[24] As explained in section 4, it is possible to infer the electron density and the conductivity at the effective height of each location. In Figure 6 they have been plotted together with the corresponding Neutral density obtained from MSIS model, for the same time span than in Figure 5. These parameters are displayed here as possible outcomes of our method but their variations will not be discussed in this paper.

## 6. Discussion

[25] It is the first time that the cut-off frequency, and its corresponding reflection height, are extensively inferred for ocean areas, and therefore there exist no previous results to compare with. International Reference Ionosphere (IRI) models [Rawer *et al.*, 1978] do not contain much information about D and E regions, as stated by *Bilitza and Reinisch* [2007]. The information used to build the models is mainly

based on incoherent scatter radar systems and data from rockets. Thus, the information is reduced to a very small set of land areas, and no data from ocean is available. Because of that, we could not establish relations between our results and IRI. We calculated the effective reflection height maps for each month (2006–2009) based on models IRI (to obtain the electron density profile) and MSIS (to obtain the neutral density profile). From them we obtained the altitude at which the condition from equation (2) is satisfied. In Figure 7 the results for the year 2006 are depicted. Other years yield similar maps. All the calculations are made at 22.30 LT, the time at which DEMETER gathers data. It can be observed that the models do not contain information about the seasonal shifts detected in our measurements. It is also interesting to note that the model predicts total shifts of no more than 3–4 km, while the maps from Figure 3 contain shifts greater than 10 km.

[26] The most prominent effect observed over the cut-off frequency occurs over the Pacific Ocean at the South Hemisphere, and has a seasonal dependence (see Figure 4). During the southern cold season (May–September) the cut-off frequency decreases on average around 200 Hz, corresponding to an effective height change of 10–12 km. The cut-off frequency is higher (around 150 Hz more) during all seasons for low latitudes. This latitudinal gradient is maintained along the seasonal shifts. Due to its seasonal nature, we believe that this shift can be originated either by the change in solar irradiation or changes in the thunderstorm activity in the region.

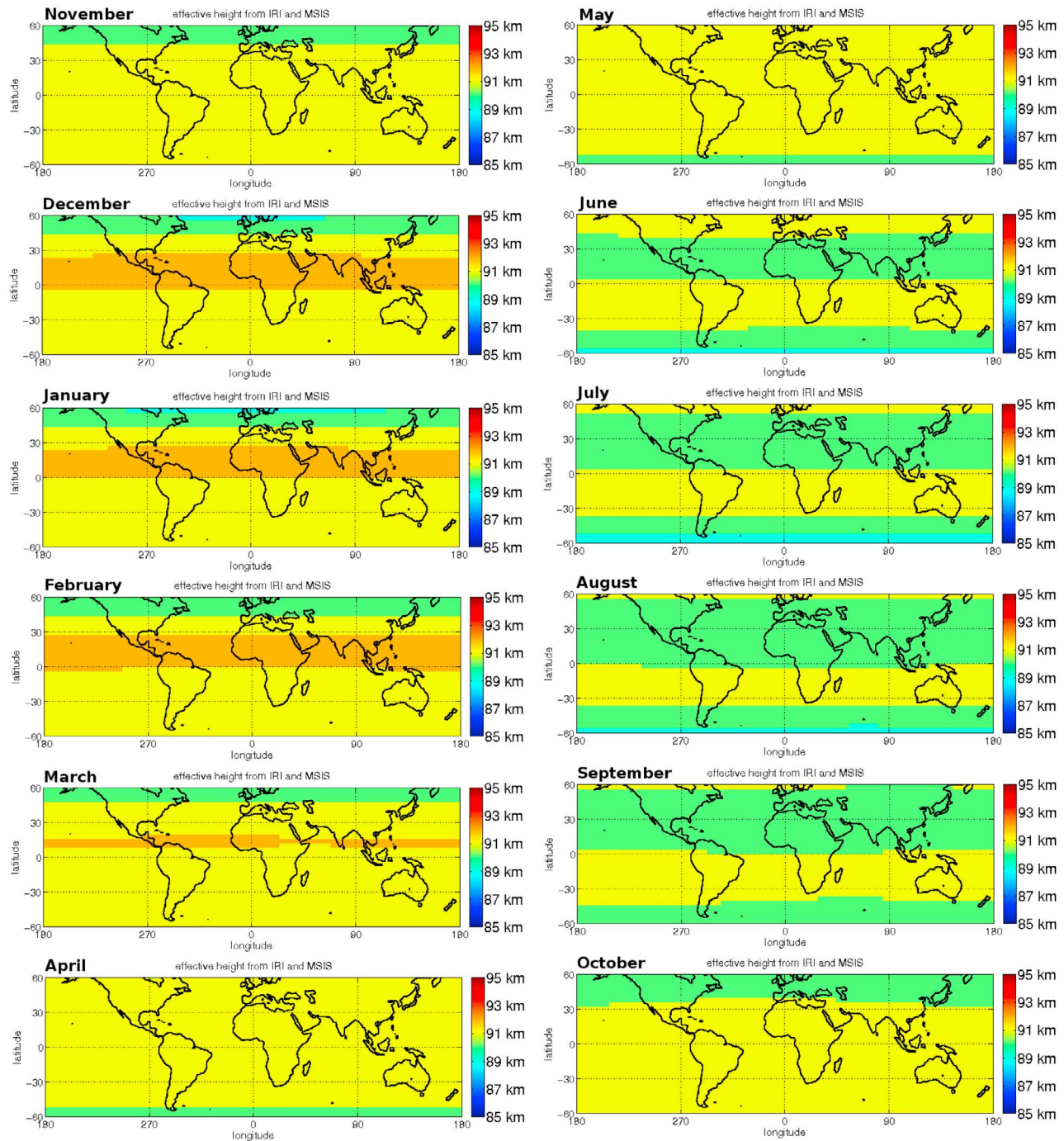


**Figure 7.** Map of the effective reflection height for each month of year 2006. Other years (2007–2009) yield similar maps. Each height (in km) is calculated at 22.30 LT, in order to compare it with DEMETER data. It has been calculated from IRI + MSIS models; the first provides the electron density profile and the second the neutral density profile for a given time and location. From them, the height which satisfies the condition of equation (2) is inferred. The altitude resolution of the plot is 1 km.

[27] A similar effect is observed over Atlantic and Indian Oceans. In this case, the seasonal shift is limited to low latitudes ( $\pm 15^\circ$  from magnetic equator). These shifts also seem to respond to a seasonal schedule, but on a semi-annual basis (see Figure 3). The maxima cut-off are registered in March–April and again in September–October. As we commented before, the Atlantic area where this phenomenon

is observed corresponds to the inter-tropical convergence zone, where the ionosphere is highly variable and presents a maximum of plasma bubbles, so these results must be taken with caution, since DEMETER may be registering other phenomena superimposed to the spectra.

[28] The observed shifts occur predominantly, although not sharply limited to, over the ocean. Certainly we do not

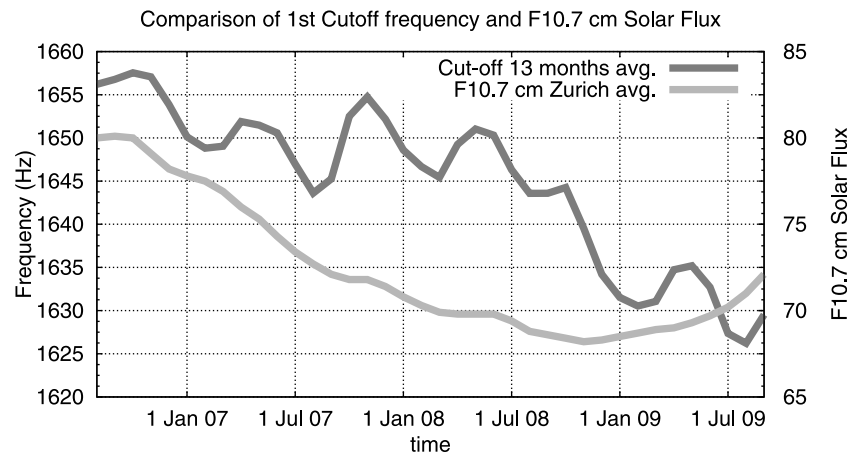


**Figure 8.** Comparison of F10.7 cm solar flux and global cut-off frequency detected by DEMETER. The global cut-off is calculated each month for the entire globe (latitude  $\pm 60^\circ$ ) and then a 13-month running average is plotted, in order to minimize seasonal effects. F10.7 cm solar flux index is also a 13-month running average, documented by *Waldmeier* [1961].

have a clear explanation for that, but we can mention several hypotheses to explain this difference:

[29] 1. It is known that aerosols have an effect on the global electric circuit (for the definition of the global electric circuit, see for example the review by *Rycroft et al.* [2000] and *Williams* [2009]). The values of the electric field in the global circuit differ between ocean and land measurements and this discrepancy is attributed to differences in aerosol and associated air conductivity [*Harrison*, 2004]. This result is due to polluted conditions over land [*Israel*, 1973a, 1973b]. This effect can change the current in the global electric circuit and may affect the cut-off frequency. Another possibility is the effect that sea salt aerosols can have over the atmosphere [*Satheesh and Moorthy*, 2005]. Large clouds of this kind of aerosol can induce modifications of the electrical properties of the Earth ionosphere waveguide. This possibility would also explain why the frontiers of the cut-off frequency shift are not sharply related to the coast line in general. There is one place where the border of the shift roughly coincides with the coast line (see Figure 5, bottom); the western coast of South-America. Along this coast line is the Andes Cordillera, which is a natural barrier for wind and therefore for aerosols [*Husar et al.*, 2000].

[30] 2. The effect of the thunderstorm activity because it is known that the occurrence of thunderstorms is less important above oceans than above land [*Christian et al.*, 2003]. This cannot be an artifact in our detection method because this method is independent of the number of whistlers. But the thunderstorm activity also modifies the global electric circuit. Using a model, *Pasko et al.* [1997] claimed that positive cloud to ground (+CG) discharges can lead to large electric fields and to the removal of large quantities of charge from ionospheric altitudes (see also *Pasko et al.* [1998], *Füllekrug* [2004], and the review paper by *Inan et al.* [2010]). However, *Rycroft et al.* [2007] concluded that the contribution of +CG or -CG strokes to the global electric circuit is not significant relative to conduction and convection currents associated with electrified thunderclouds to maintaining the ionospheric potential. It remains that the

electron density at the bottom of the ionosphere can be globally different above oceans and above land because thunderstorms are not so numerous above oceans.

[31] 3. The effect of some Transient Luminous Events (TLE) due to powerful lightning strokes. A simulation of the effect of these strokes has been made by *Rodger et al.* [2001] which shows increases in the electron density of the lower ionosphere, with the largest increases at 90 km altitude. The study carried out by *Mende et al.* [2005] indicates that elves can ionize the upper atmosphere and that it could be a significant source of ionization in the low- to mid-latitude nighttime D region. Later on, *Chen et al.* [2008] have shown that occurrence of elves is much more important above oceans than above land. They also determined that the total electron content at the lower ionosphere above elve hot zones can be increased by more than 5%. This can also contribute to a decrease of the bottom altitude of the ionosphere over oceans.

[32] Since the electromagnetic source for the excitation of the cavity is lightning, our results must contain information about the global lightning patterns as well. In the study by *Gemelos et al.* [2009], the spectral electric field intensity in the range of 5–10 kHz (measured by DEMETER) is related to energetic electron precipitation due to lightning. Their results are in good agreement with our maps for the different seasons. By observing their seasonal maps it can be noticed that an increase on electric field intensity on the mentioned range corresponds to a decrease of the cut-off frequency and vice versa.

[33] The reported shifts on the cut-off frequency show the variation of the effective height of the Earth-ionosphere waveguide, directly related in equation (1) [*Cheng*, 1989]. This height depends on the varying refractive index of wave propagation in magneto active plasma, expressed by the Appleton-Hartree formula [*Budden*, 1961], which depends mainly on the electron density profile as well as on the density of neutrals. If we neglect the effect of the Earth's magnetic field on the ionospheric plasma, the reflection occurs when  $f_p^2 = f\nu$ , as stated in section 4. Thus, it is

possible to extract the electron density as well as the conductivity at the detected effective reflection height, by using neutral density data from a model like MSIS.

[34] By looking at Figure 4, it can be noticed that there is a general decrease of the cut-off frequency over the four years. It can be observed at northern cold season plots, for ocean areas near the geomagnetic equator. Winter plots at these areas show decreasing average values for the cut-off frequency from 2006 to 2009. We explain this behavior due to the decreasing solar activity (measured by means of F10.7 index) along these years, extensively reported by *Solomon et al.* [2011]. Lower solar activity implies lower electron density at the ionosphere, thus increasing the effective height of the ionosphere and lowering the cut-off frequency. In order to confirm that, we calculated the global average value (all valid points between  $\pm 60^\circ$  latitude) of the effective height for each month of 2006–2009. Then a 13-month running average was computed in order to minimize the seasonal effects described above. In Figure 8, this result is compared with the 13-month Zurich average [*Waldmeier*, 1961] of the F10.7 cm solar flux parameter. It can be observed that during the major part of the time span both parameters decrease, except for the last six months where the solar flux parameter starts increasing. The ripple of the average cut-off frequency curve is caused by the seasonal patterns described above.

## 7. Conclusion

[35] A large data set of electric field measurements from DEMETER has been employed to draw average maps of the effective reflection height with dependence of geolocation. There exist previous works which use the cut-off frequency to calculate the effective height of the Earth-ionosphere cavity from ground observations [*Ohya et al.*, 2006; *Kumar et al.*, 2009; *Ostapenko et al.*, 2010], but it was never done before, to the knowledge of the authors, by using data taken from spacecraft. This technique has the clear advantage of monitoring most of the surface of Earth. Ground based studies of the cut-off frequency can only give averaged values along the path that the atmospheric wave followed (from source to point of observation), while measurements at the satellite are directly related to the ionosphere conditions in the vicinity of the measurement point. Thus, we present detailed maps (up to  $2^\circ$  resolution) over the whole Earth ( $\pm 60^\circ$  latitude) for the effective reflection height of the ionosphere or the D-region altitude, which is inversely proportional to the cut-off frequency. From these measurements, it is possible to infer the electron density as well as the conductivity at the effective height, although it is necessary to extract the neutral density parameter from a model, MSIS in this case.

[36] The main result of this study is that we observe, during nighttime, an increase of the cut-off frequency of the Earth-ionosphere waveguide over oceans during northern cold season. This corresponds to a decrease of the effective height of the ionosphere.

[37] **Acknowledgments.** This work was supported by the Centre National d'Etudes Spatiales, the Ministerio de Ciencia e Innovación of Spain and Consejería de Innovación, Ciencia y Empresa of Andalusian Government under projects with references FIS2010-15170 and PO7-FQM-03280, co-financed with FEDER funds of the European Union. It is

based on observations with the electric field experiment ICE embarked on DEMETER. The authors thank J.J. Berthelier, the Principal Investigator of ICE for the use of the data. IRI model used in this work was taken from <http://nssdcftp.gsfc.nasa.gov>, and MSIS model was taken from <ftp://hanna.cmc.gsfc.nasa.gov>. The authors want to thank to all the developers and maintainers for the availability of these tools. We are also grateful for the availability of data from F10.7 solar flux parameter, obtained from <http://sail.msfc.nasa.gov>. Finally the authors thank the referees for their valuable comments to improve the quality of the paper.

[38] Robert Lysak thanks Alexander Nickolaenko and another reviewer for their assistance in evaluating this paper.

## References

- Barr, R., D. L. Jones, and C. J. Rodger (2000), ELF and VLF radio waves, *J. Atmos. Sol. Terr. Phys.*, *62*, 1689–1718.
- Berthelier, J., et al. (2006), ICE, the electric field experiment on DEMETER, *Planet. Space Sci.*, *54*(5), 456–471, doi:10.1016/j.pss.2005.10.016.
- Bilitza, D., and B. W. Reinisch (2007), International reference ionosphere 2007: Improvements and new parameters, *Adv. Space Res.*, *42*, 599–609.
- Bliokh, P. V., Y. P. Galyuk, E. M. Hänninen, A. P. Nickolaenko, and L. M. Rabinovich (1977), Resonance effects in the Earth-ionosphere cavity, *Inst. Radiophys. Electr.*, *20*(4), 501–509.
- Budden, K. G. (1961), *Radio Waves in the Ionosphere*, Cambridge Univ. Press, Cambridge, UK.
- Chen, A. B., et al. (2008), Global distributions and occurrence rates of transient luminous events, *J. Geophys. Res.*, *113*, A08306, doi:10.1029/2008JA013101.
- Cheng, D. K. (1989), *Field and Wave Electromagnetics*, Addison-Wesley, Reading Mass.
- Christian, H. J., et al. (2003), Global frequency and distribution of lightning as observed from space by the Optical Transient Detector, *J. Geophys. Res.*, *108*(D1), 4005, doi:10.1029/2002JD002347.
- Cummer, S. A. (2000), Modeling electromagnetic propagation in the Earth-ionosphere waveguide, *IEEE Trans. Antennas Propag.*, *48*(9), 1420–1430.
- Cummer, S. A., U. S. Inan, and T. F. Bell (1998), Ionospheric D region remote sensing using VLF radio atmospherics, *Radio Sci.*, *33*(6), 1781–1792.
- Cussac, T., M.-A. Clair, P. Ultré-Guerard, F. Buisson, G. Lassalle-Balier, M. Ledu, C. Elisabelar, X. Passot, and N. Rey (2006), The DEMETER microsatellite and ground segment, *Planet. Space Sci.*, *54*(5), 413–427, doi:10.1016/j.pss.2005.10.013.
- Füllekrug, M. (2004), The contribution of intense lightning discharges to the global atmospheric electric circuit during April 1998, *J. Atmos. Sol. Terr. Phys.*, *66*, 1115–1119.
- Gemelos, E. S., U. S. Inan, M. Walt, M. Parrot, and J. A. Sauvaud (2009), Seasonal dependence of energetic electron precipitation: Evidence for a global role of lightning, *Geophys. Res. Lett.*, *36*, L21107, doi:10.1029/2009GL040396.
- Hargreaves, J. K. (1992), *The Solar-Terrestrial Environment*, Cambridge Univ. Press, New York.
- Harrison, R. G. (2004), The global atmospheric electrical circuit and climate, *Surv. Geophys.*, *25*, 441–484.
- Hayakawa, M., K. Ohta, and K. Baba (1994), Wave characteristics of tweek atmospherics deduced from the direction-finding measurement and theoretical interpretation, *J. Geophys. Res.*, *99*, 10,733–10,743.
- Hedin, A. E. (1991), Extension of the MSIS Thermospheric model into the middle and lower atmosphere, *J. Geophys. Res.*, *96*, 1159–1991.
- Husar, R. B., J. D. Husar, and L. Martin (2000), Distribution of continental surface aerosol extinction based on visual range data, *Atmos. Environ.*, *34*, 5067–5078.
- Inan, U. S., S. A. Cummer, and R. A. Marshall (2010), A survey of ELF and VLF research on lightning-ionosphere interactions and causative discharges, *J. Geophys. Res.*, *115*, A00E36, doi:10.1029/2009JA014775.
- Israel, H. (1973a), *Atmospheric Electricity*, vol. 1, *Fundamentals, Conductivity, and Ions*, Isreal Prog. Sci. Transl., Springfield, Va.
- Israel, H. (1973b), *Atmospheric Electricity*, vol. 2, *Fields, Charges, and Currents*, Isreal Prog. Sci. Transl., Springfield, Va.
- Kil, H., and R. A. Heelis (1998), Global distribution of density irregularities in the equatorial ionosphere, *J. Geophys. Res.*, *103*, 407–417.
- Kumar, S., A. Deo, and V. Ramachandran (2009), Nighttime D-region equivalent electron density determined from tweeks sferics observed in the south pacific region, *Earth, Planets Space*, *61*, 905–911.
- Labitzke, K., J. J. Barnett, and B. Edwards (1985), *Handbook MAP 16, SCOSTEP*, Univ. Ill., Urbana, Ill.
- Lagoutte, D., J. Y. Brochot, D. de Carvalho, L. Madrias, and M. Parrot (2005), DEMETER microsatellite scientific mission center data product

- description, *Tech. Rep. DMT-SP-9-CM-6054-LPC*, Lab. de Phy. et Chim. de l'Environ. et de l'Espace, Orléans, France.
- Lagoutte, D., et al. (2006), The DEMETER science mission centre, *Planet. Space Sci.*, *54*(5), 428–440, doi:10.1016/j.pss.2005.10.014.
- Lazebny, B. V., A. P. Nickolaenko, V. A. Rafalsky, and A. V. Shvets (1988), Detection of transverse resonances of the Earth-ionosphere cavity in the average spectrum of VLF atmospherics, *Geomagn. Aeron.*, *28*(2), 281–282.
- Mende, S. B., H. U. Frey, R. R. Hsu, H. T. Su, A. B. Chen, L. C. Lee, D. D. Sentman, Y. Takahashi, and H. Fukunishi (2005), D region ionization by lightning-induced electromagnetic pulses, *J. Geophys. Res.*, *110*, A11312, doi:10.1029/2005JA011064.
- Nickolaenko, A. P., and M. Hayakawa (2002), *Resonances in the Earth-Ionosphere Cavity*, Kluwer Acad., Dordrecht, Netherlands.
- Ohya, H., M. Nishino, Y. Murayama, and K. Igarashi (2003), Equivalent electron densities at reflection heights of tweek atmospherics in the low-middle latitude D-region ionosphere, *Earth, Planets Space*, *55*(10), 627–635.
- Ohya, H., M. Nishino, Y. Murayama, K. Igarashi, and A. Saito (2006), Using tweek atmospherics to measure the response of the low-middle latitude D-region ionosphere to a magnetic storm, *J. Atmos. Sol. Terr. Phys.*, *68*, 697–709.
- Onishi, T., and J. J. Berthelier (2010), Synthetic characterization of VLF electric field spectra from the ICE experiment on DEMETER automatic recognition and characterization of natural and man made emissions, *Technical report*, Inst. Pierre Simon Laplace, Paris.
- Ostapenko, A. A., E. E. Titova, A. P. Nickolaenko, J. M. T. Turunen, and T. Raita (2010), Characteristics of VLF atmospherics near the resonance frequency of the Earth-ionosphere waveguide 1.6–2.3 kHz by observations in the auroral region, *Ann. Geophys.*, *28*, 193–202.
- Pasko, V. P., U. S. Inan, T. F. Bell, and Y. N. Taranenko (1997), Sprites produced by quasi-electrostatic heating and ionization in the lower ionosphere, *J. Geophys. Res.*, *102*(A3), 4529–4561, doi:10.1029/96JA03528.
- Pasko, V. P., U. S. Inan, and T. F. Bell (1998), Ionospheric effects due to electrostatic thundercloud fields, *J. Atmos. Sol. Terr. Phys.*, *60*, 863–870.
- Ramo, S., J. R. Whinnery, and T. V. Duzer (1994), *Fields and Waves in Communication Electronics*, 3rd ed., 409 pp., John Wiley, New York.
- Ratcliffe, J. A. (1959), *The Magneto-Ionic Theory and its Applications to the Ionosphere*, Cambridge Univ. Press, London.
- Rawer, K., D. Bilitza, and S. Ramakrishnan (1978), Goals and status of the International Reference Ionosphere, *Rev. Geophys.*, *16*, 177–181.
- Rodger, C. J., M. Cho, M. A. Clilverd, and M. J. Rycroft (2001), Lower ionospheric modification by lightning-EMP: Simulation of the night ionosphere over the United States, *Geophys. Res. Lett.*, *28*(2), 199–202, doi:10.1029/2000GL011951.
- Ryabov, B. S. (1992), Tweek propagation peculiarities in the Earth-ionosphere waveguide and low ionosphere parameters, *Adv. Space Res.*, *12*(6), 255–258.
- Rycroft, M. J., S. Israelsson, and C. Price (2000), The global atmospheric electric circuit, solar activity and climate change., *J. Atmos. Sol. Terr. Phys.*, *62*, 1563–1576.
- Rycroft, M. J., A. Odzimek, N. F. Arnold, M. Füllekrug, A. Kułak, and T. Neubert (2007), New model simulations of the global atmospheric electric circuit driven by thunderstorms and electrified shower clouds: The roles of lightning and sprites, *J. Atmos. Sol. Terr. Phys.*, *69*, 2485–2509.
- Satheesh, S. K., and K. K. Moorthy (2005), Radiative effects of natural aerosols: A review, *Atmos. Environ.*, *39*(11), 2089–2110.
- Schumann, W. O. (1952), Über die strahlungslosen eigenschwingungen einer leitenden kugel, die von einer luftschicht und einer ionosphärenhülle umgeben ist, *Z. Naturforsch. A*, *7*(2), 149–154.
- Shvets A. V., and M. Hayakawa (1997), Polarisation effects for tweek propagation, *J. Atmos. Sol. Terr. Phys.*, *60*(44), 461–469.
- Solomon, S. C., L. Qian, L. V. Didkovsky, R. A. Viereck, and T. N. Woods (2011), Causes of low thermospheric density during the 2007–2009 solar minimum, *J. Geophys. Res.*, *116*, A00H07, doi:10.1029/2011JA016508.
- Su, S. Y., C. H. Liu, H. H. Ho, and C. K. Chao (2006), Distribution characteristics of topside ionospheric density irregularities: Equatorial versus midlatitude regions, *J. Geophys. Res.*, *111*, A06305, doi:10.1029/2005JA011330.
- Taflove, A., and S. C. Hagness (2005), *Computational Electrodynamics, the Finite-Difference Time Domain method*, 3rd ed., Artech House, Norwood, Mass.
- Toledo-Redondo, S., et al. (2010), Study of Schumann resonances based on magnetotelluric records from the western Mediterranean and Antarctica, *J. Geophys. Res.*, *115*, D22114, doi:10.1029/2010JD014316.
- Waldmeier, M. (1961), *The Sunspot Activity in the Years 1610–1960*, Schulthess, Zurich, Switzerland.
- Williams, E. R. (1992), The Schumann resonance: A global tropical thermometer, *Science*, *256*, 1184–1187.
- Williams, E. R. (2009), The global electrical circuit: A review, *Atmos. Res.*, *91*, 140–152, doi:10.1016/j.atmosres.2008.05.018.

M. Parrot and S. Toledo-Redondo, Laboratoire de Physique et Chimie de l'Environnement et de l'Espace, CNRS, 3A Ave. de la Recherche Scientifique, F-45071 Orléans CEDEX 2, France. (sergiotr@ugr.es)  
 A. Salinas, Department of Electromagnetism and Matter Physics, University of Granada, Av. Severo Ochoa, E-18071 Granada, Spain.